Catalytic Degradation of Organic Dyes Dissolved in Aqueous Solutions by Electro-Fenton Process

Submitted by
Md. Yeasin Pabel
M.S. Research Fellow
Bose Center for Advanced Study and Research in Natural Sciences
University of Dhaka, Dhaka-1000, Bangladesh

Supervised by
Dr. Md. Mominul Islam
Professor
Department of Chemistry
University of Dhaka, Dhaka-100000, Banglades

Director
Bose Centre for Advanced Study & Research
Dhaka University

ABSTRACT. In recent days, manganese dioxide (MnO_2) and polyaniline (PAni) nanocomposites have intrigued material science researches extensively due to its wide range of applications. In this study, the preparation of MnO_2 nanoparticles and PAni nanocomposites by ultrasonication process is reported. The MnO_2 nanoparticles were prepared by hydrothermal treatment of the mixed solution by an autoclave reactor at low temperature. PAni was synthesized by chemical oxidative polymerization using $(NH_4)_2S_2O_8$ as oxidizing agent in acidic condition. Successful formations of the materials and composites were characterized with X-ray diffraction (XRD), transmission electron microscopy (TEM), Fourier transform-infrared (FT-IR) spectroscopy, and Thermogravimetric analysis (TGA). The MnO_2 particles produced were α-MnO_2 with a rod-like morphology and a size of approximately 37 nm. Fourier transform infrared spectra shows that a peak around 1142 cm^{-1} is the characteristic peak for the conductivity of PAni. A new at 952 cm^{-1} arises for the MnO_2/PAni composites demonstrates that some special interaction exists between MnO_2 and PAni. The composite obtained hopefully will exhibit excellent electrocatalytic activity toward the oxygen reduction reaction following a two-electron transfer mechanism.

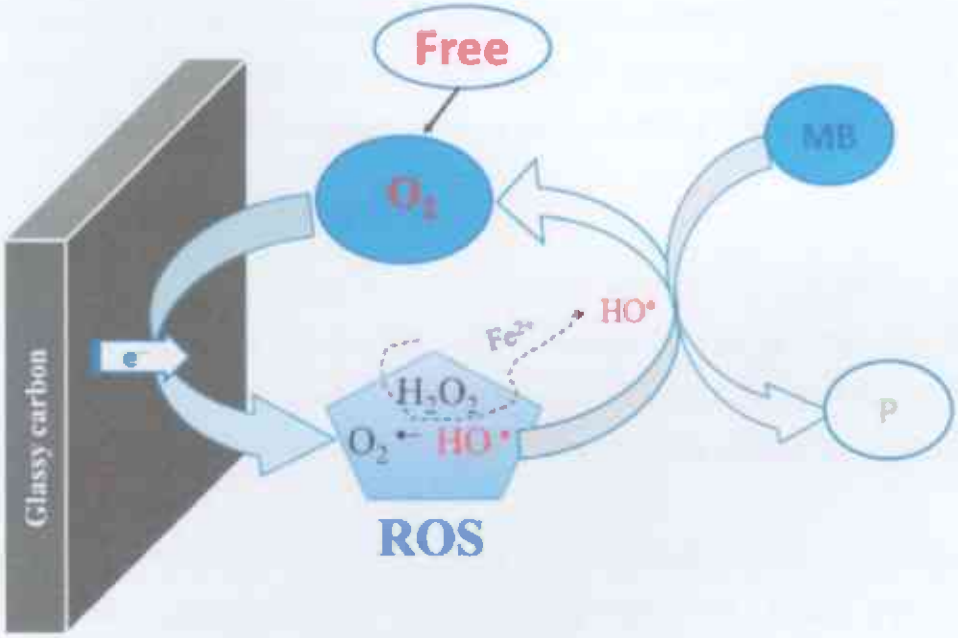
INTRODUCTION

Environmental pollution has increased dramatically in recent decades as a result of enormous industrialization [1]. One of the worst environmental pollutions is the entry of organic dyes into surface water. Dye is a common colorant in the textile, pulp, rubber, plastic, printing, pharmaceutical, and food sectors. Synthetic organic dyes are especially common. In essence, these sectors use more than 30,000 commercial colors based on 8,000 different chemical structures, some of which are discharged with industrial effluent [2]. Both groundwater and surface water contain the majority of them, which are permanent. The scientific community is now paying increasing attention to water contamination since it has major effects on ecosystems as well as humans [3]. Consequently, it is crucial to treat wastewater containing color, particularly that from the textile sector, in order to protect our environment.

Advanced oxidation processes (AOPs), among the different techniques employed [4], exhibit encouraging potential for the treatment of wastewater containing organic dyes due to their significant unique benefits [4]. AOPs effectively break down organic dyes into a variety of gaseous, ionic, or neutral components that are thought to be non-toxic to aquatic life. Hydroxyl radical ($OH^{\bullet}$) is by far the most advantageous oxidant among those employed to treat wastewater

because of its variety of special characteristics [4]. Organic substances can be broken down by $OH^{\bullet}$, and since it has a brief radical life, secondary contamination is eliminated. These two combined properties have led to the rapid development of AOPs that rely on free radical chemistry to decompose/mineralize organic pollutants in water and wastewater. The $OH^{\bullet}$ radicals produced by AOPs either oxidize complex organic species into smaller organic fragments or are completely mineralized to CO_2 and H_2O. The conventional Fenton reaction produces highly oxidizing $OH^{\bullet}$ from hydrogen peroxide (H_2O_2) and iron (II) ions (Fe^{2+}) [4]. Despite its ability to remove virtually all organic pollutants, the original Fenton process involves the use of H_2O_2 and Fe^{2+}, which makes the process costly for large applications [4]. In addition, the use of Fe^{2+} causes secondary pollution (*i.e.*, iron residue in the form of paint in wastewater or ferric sludge, both of which require further treatment).

To address these shortcomings, electro-Fenton (EF) has been extensively studied for the purpose of *in-situ* generation of reactive oxygen species (ROS) ($O_2^{\bullet-}$, $OH^{\bullet}$, H_2O_2) [4-6], cathode regeneration of Fe^{2+}, or a combination of both as represented in Scheme 1.



Scheme 1. Schematic diagram of *in-situ* generation of reactive oxygen species in electro-Fenton process [5].

The ORR can be catalyzed by a variety of TMO-based catalysts, however MnO_2 stands out for being readily available, inexpensive, and capable of catalysis. The activity and selectivity of

MnO_2 towards ORR is regulated by a variety of parameters including size, shape, crystal structures [7]. However, due to its low electrical conductivity and low adhesion with electrode, polymer materials such as polypyrrole, polythiophene, polyaniline, or poly(vinyl alcohol) have been applied to confront these difficulties as well as to hasten the ORR process [8]. PAni has been seen as the most appealing polymer among the other conductive polymers studied due to its low cost, redox property, good conductivity, and environmental stability [8]. Moreover, PAni exhibits electrocatalytic selectivity and activity towards H_2O_2 production. Therefore MnO_2/PAni composites are versatile and promising ORR catalysts since the dispersion phase and matrix phase may be tuned to produce sites for preferred O_2 adsorption direction. PAni has been largely explored as a matrix phase in Mn_xO_y/PAni composites for several purposes, including ORR catalysis [8, 9]. MnO_2/PAni composites, in which PAni may be employed as a dispersed phase, have not undergone much research for ORR yet.

In this report, MnO_2, PAni, and MnO_2/PAni nanocomposites were prepared *via* hydrothermal, chemical oxidative polymerization, and ultrasonication method. Following the successful preparation of materials and nanocomposites, the samples were characterized using relevant sophisticated techniques. The use of cheap, stable and scalable materials indicates high commercial feasibility for the applications in water and wastewater remediation.

EXPERIMENTAL

Chemicals. Analytical grade chemicals and materials such as $KMnO_4$ (Sigma, Germany), $MnSO_4.H_2O$ (Sigma, Germany), C_6H_5-NH_2 (Merck, India), HCl (RCI, Thailand), $(NH_4)_2S_2O_8$ (APS), (PanreacQuimica, SAU, Spain), H_2SO_4 (Merck, Germany). All aqueous solutions were prepared with deionized (DI) water (specific conductivity of 0.055 µS/cm, Model: BOECO pure, BOE-8082060, Germany).

Characterization of Materials. Fourier transform-infrared (FT-IR) spectra were recorded with a Fourier Transform Spectrophotometer by Frontier FT-NIR/MIR, Perkin Elmer, USA in transmittance mode. The X-ray diffraction (XRD) pattern of the samples were recorded with PANalytical X'Pert Pro diffractometer (Philips PW 1724) operating at 40 kV and 30 mA using Cu $K\alpha_1$ fitted with scintillation detector. Transmission electron micrographs were obtained with Transmission Electron Microscopy (TEM); JEM-2100F operated at 200kV FE (Field Emission) accelerating voltage; Tokyo, Japan.

Preparation of Catalysts. The synthesis of α-MnO_2 was divided into two steps: Preparation of precursor solution and hydrothermal treatment of the mixed solution by an autoclave reactor at low temperature (Scheme 2). $KMnO_4$ and $MnSO_4.H_2O$ were mixed in sufficient DI water with molar ratio of 1:1.87.



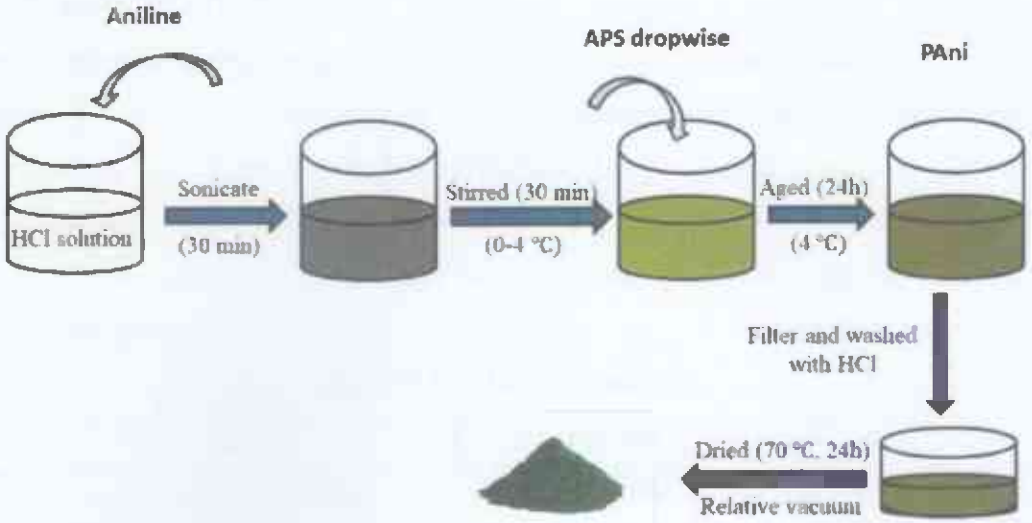
Scheme 2. A schematic showing hydrothermal synthesis of α-MnO_2.

Afterwards, the mixture was subjected to sonication for about 30 min. Finally, the suspension was transferred to a Teflon lined stainless steel autoclave and heated at 140 °C for 12 h in a muffle furnace. The overall reaction is

$$2KMnO_4 + 3MnSO_4 + 2H_2O \rightarrow 5MnO_2 + K_2SO_4 + 2H_2SO_4 \quad (2.1)$$

The product was finally washed with DI water several times and dried in an oven at 80 °C.

Scheme 3 depicts the chemical oxidative polymerization (COP) process used to prepare PAni. A monomer solution was prepared by adding aniline monomer into 1 M HCl. Next, APS powder was mixed with 1 M HCl solution to form the initiator solution. Monomer and initiator solutions were then simultaneously dropped into a reactor glass, and the mixture was stirred for 8 h at 5 °C. The product was then washed with DI water several times and dried in an oven at 60 °C for 24 h.



Scheme 3. Schematic representation of COP of aniline monomer using APS as redox initiator.

MnO_2/PAni nanocomposites varying the percentage of PAni were prepared by solution sonication method. Required amount of MnO_2 and PAni were dispersed into ethanol. Afterwards, the suspensions were subjected to sonication for about 2 h. The composite was then dried in room temperature for 24 h. The percentage of PAni in the nanocompoite is tabulated in Table 1.

Table 1 Abbreviated name of the prepared composites.

Composite	Abbreviation (MnO_2/PAni - X)
MnO_2 with 10% PAni	MnO_2/PAni–10
MnO_2 with 15% PAni	MnO_2/PAni–15
MnO_2 with 20% PAni	MnO_2/PAni–20

RESULTS AND DISCUSSION

Characterization of the Materials. As described in the experimental sections, α–MnO_2 and PAni and their composites were synthesized by following different experimental conditions and using different composition of precursors. The methods and experimental conditions of synthesis of materials are summarized in Table 2. However, among these materials synthesized the detailed characterizations of α–MnO_2 and α–MnO_2/PAni-20 nanocomposites were typically carried out and are described as follows.

Table 2 Synthesis of catalysts.

Material	Method	Precursors and experimental conditions
α–MnO_2	Hydrothermal	$KMnO_4$; $MnSO_4.H_2O$; HCl; 140 °C; 12 h
PAni	Chemical oxidative polymerization	Aniline; APS; HCl; 0-4 °C; stirring for 8 h
MnO_2/PAni	Ultrasonication method	α–MnO_2; and PAni; ethanol; 2 h sonication

XRD patterns of MnO_2 and MnO_2/PAni are shown in Figure 1. The diffraction patterns of the sample as a whole are all well indexed to the tetragonal symmetry α–MnO_2 with a space group of *I*4/m and are in good accord with the standard values of JCPDS card No. 440141 [10].

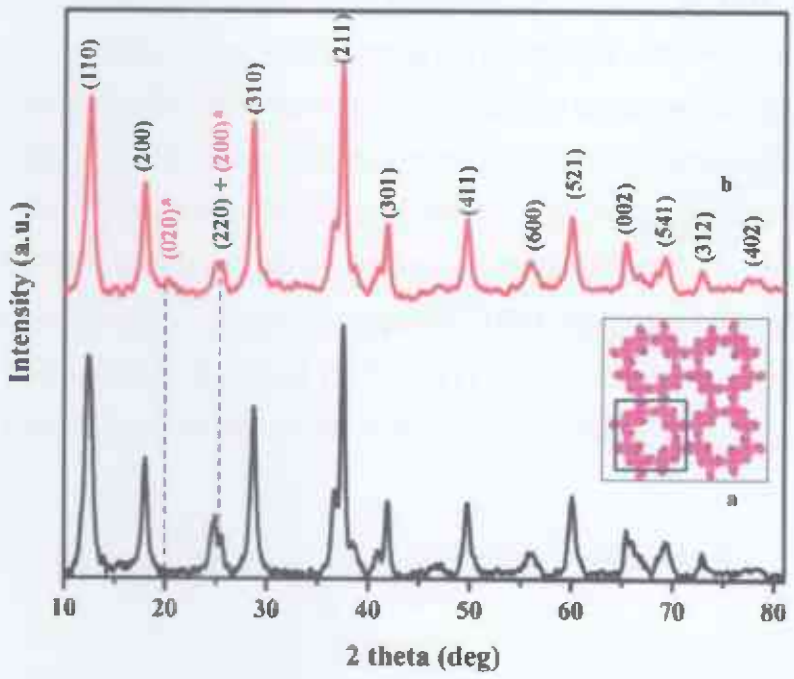


Figure 1. XRD patterns of (a) α–MnO_2 nanowire and crystallographic structure (inset) of α–MnO_2, and (b) MnO_2/PAni-20 nanocomposites. Asterisk (*) corresponds peaks of pure PAni.

The sample is of pure form because there is no sign of any other phases. The average crystallite size (d) of the α–MnO_2, calculated from the width of (211) peak using the *Scherrer formula*, $d = 0.9\lambda/\beta_{1/2}\cos\theta$ (where λ is the X-ray wavelength, $\beta_{1/2}$ is the corrected width of the main diffraction peak at half height and θ is the diffraction angle) was 37 nm. As seen in the inset of Figure 1a, the α–MnO_2 has a [2 × 2] tunnel structure. Therefore, it is clear that the synthesized material is α–MnO_2. The pristine PAni generally exhibits one sharp peak centered around 25.3° accompanied by another low intensity peak with position around 20°, corresponding to (200), and (020) semicrystalline planes, respectively, of PAni in its emeraldine salt (ES) form [11]. However in MnO_2/PAni-20, a slight change of (220) peak of pure MnO_2 occurred due to overlaping of (200) peak of PAni and a low intensity peak with position 20° corresponding to (020) plane of PAni is observed. These findings show that PAni is present in the prepared MnO_2/PAni nanocomposites.

TEM were used to study the morphology of the α–MnO_2 and MnO_2/PAni nanocomposite. Figure 2(A–D) and (A′–D′) shows that the TEM images of synthesized α–MnO_2 and MnO_2/PAni–20 nanocomposite. As prepared α–MnO_2 showed wire–like morphology with irregular size of length (Figure 2(A–D)). The diameter of a single nanowire of MnO_2 is about 30 nm as estimated from the TEM image (Figure 2(D)). The composite sample, MnO_2/PAni–20 shows the presence of PAni chain agglomerates on the surface MnO_2 nanowires (Figure 2(A′–D′)). Agglomeration of PAni is due to van der Waals forces. Red boxes in the Figure 2(A′–D′) indicate the adherence of PAni with MnO_2 nanowires. The distribution of the PAni is not homogeneous, because the polarity of PAni on the surface of MnO_2 leads to intermolecular attraction and chain agglomeration. Figure 2(D′) shows that there is a good contact between PAni and the MnO_2 nanowire. Figure 2(E) represents the SAED of MnO_2 which shows faint rings with bright spots that are characteristic of nanocrystalline materials. SAED patterns of the pure α–MnO_2 nanowires in Figure 2(E) also reveal bright spots that correspond to the (200), (310), (211), (301), (411), and (521) planes of the α–MnO_2 structure. These are a good agreement with the XRD result.

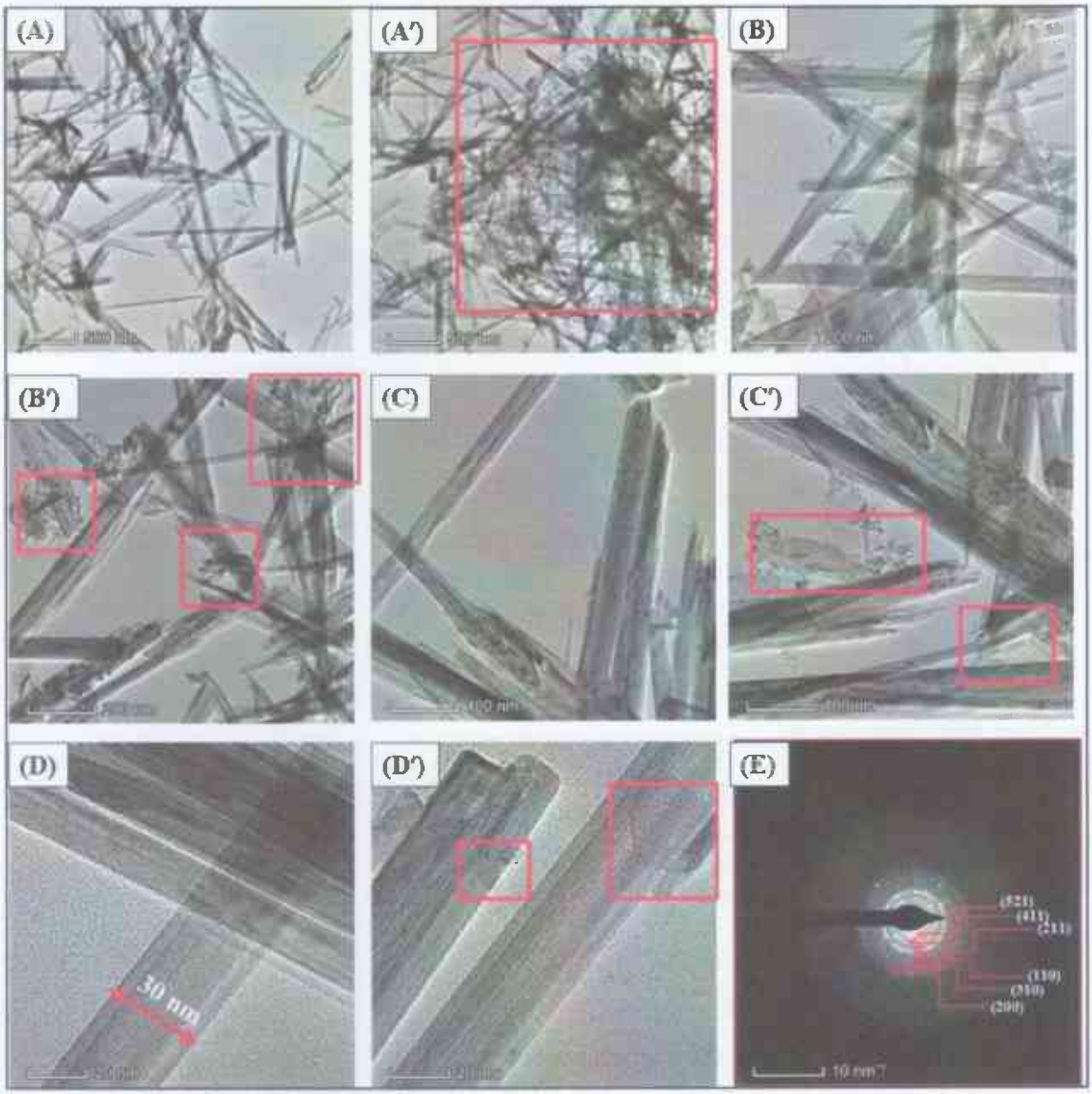


Figure 2. TEM images of (A–D) pure α–MnO_2 at different resolutions, (A′–D′) MnO_2/PAni–20 nanocomposite at the same resolutions of (A–D), and (E) Selected area electron diffraction (SAED) patterns pure α–MnO_2. Red boxes indicate adherence of PAni with MnO_2 nanowires.

FT-IR spectroscopy is renowned for its excellent sensitivity, particularly in identifying organic and inorganic compounds with trace amounts. The FT-IR spectra of synthesized pure α–MnO_2, PAni, and MnO_2/PAni–20 nanocomposite are presented in Figure 3.

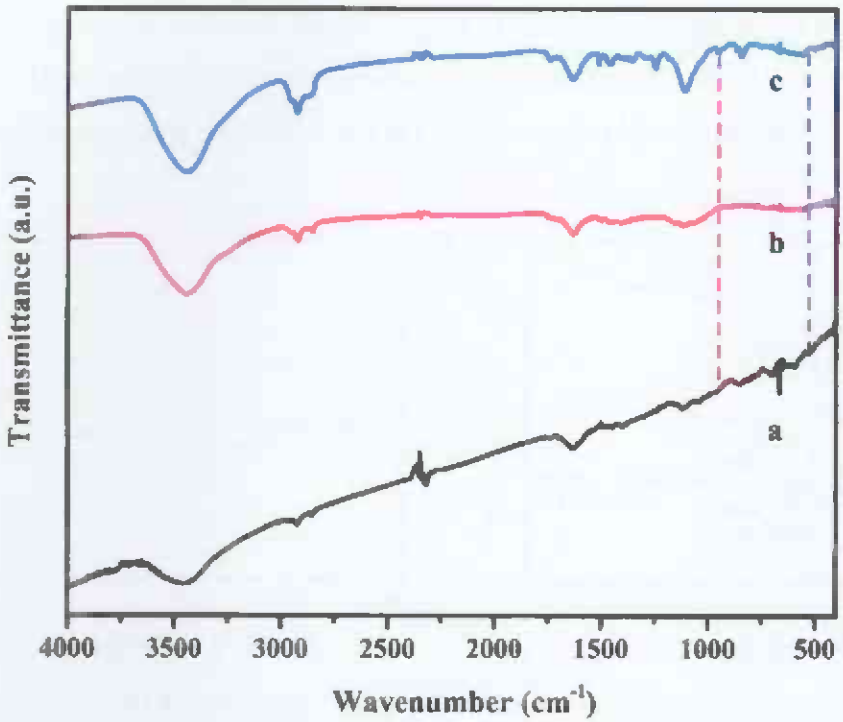


Figure 3. FT-IR spectra of (a) α–MnO_2 nanowire, (b) pure PAni, (c) MnO_2/PAni–20.

The α–MnO_2 vibrational peaks are always below 800 cm^{-1} [12]. Simplicity of the FT-IR spectrum of α–MnO_2 shown in Figure 3a again indicates its higher symmetry in structure (tetragonal α–MnO_2). The peaks below 750 cm^{-1} in Figure 3a are attributed to the Mn–O vibrations of α–MnO_2 nanowires [12]. The peaks at 1642 and 3450 cm^{-1} in the spectrum of α–MnO_2 nanowires are attributed to minute amounts of water that the nanowires had taken from their surroundings. Figure 3b shows the transmittance peaks at 1430, 1142, and 816 cm^{-1} for the vibrational mode of pure PAni. The peak around 1142 cm^{-1} is the characteristic peak for the conductivity of PAni (ES), which is also an indication of the degree of delocalization of electrons [13]. The peak at 520 cm^{-1} for MnO_2 are shifted from their standard positions in Figure 3c to a higher frequency region (see right vertical dashed line in the Figure). Interestingly, a new at 952 cm^{-1} arises for the MnO_2/PAni composite (see left vertical dashed line in Figure 3). It demonstrates that some special interaction

exists between MnO_2 and PAni [13]. This both findings, shifting and new peak, indicate that an interaction must occur between PAni and MnO_2. Thus, the FT-IR spectrum further confirms the formation of MnO_2/PAni nanocomposites.

Figure 4 displays the TG curves of as prepared (a) α–MnO_2 and (b) MnO_2/PAni–20 nanocomposite. Figure 4(A) depicts the TG curve of α–MnO_2 nanowire. At low temperatures (below 300 °C), TG curve have decreased quickly. The removal of absorbed and lattice water from the MnO_2 is the reason of this rapid decrease in the TG curve at low temperatures.

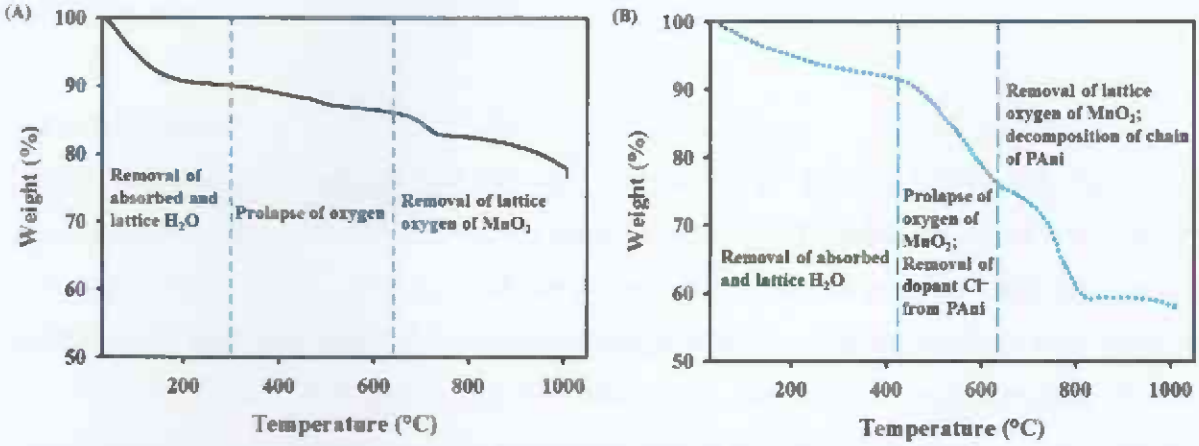


Figure 4. TG curve of (A) α–MnO_2, and (B) MnO_2/PAni–20 at N_2 gas environment with heating rate 10 °C/min at alumina pan. The samples were hold for 30 min at 1000 °C.

Between 300 and 620 °C, TG curve slowly declined, and the additional mass loss in this range is primarily ascribed to oxygen molecule prolapse. Further heating leaded to the removal of lattice oxygen, which corresponds to the subsequent occurrence of high weight loss rate [14]. The MnO_2 sample showed a weight loss of 6% up to 100 °C due to the evaporation of moisture from the surface of MnO_2 nanowires. It showed a weight loss of 16% in the temperature range of 100–1000 °C. The total weight loss of MnO_2 sample from 30 to 1000 °C was ca. 22%. The TG curve of MnO_2/PAni depicted in Figure 4(B) shows that the first stage weight loss occurs below 410 °C which is due to the loss of absorbed and lattice water from the MnO_2 [14]. In the nanocomposite removal of lattice water from MnO_2 is difficult due to the adherence of PAni on the MnO_2 surface. The second stage of weight loss between 410 to 615 °C is due to prolapse oxygen molecule of MnO_2 and removal of the dopant anion (Cl^-) contained in the PAni.

The final stage decomposition is the due to the removal of lattice oxygen of MnO_2 and decomposition of molecular chain of PAni. The MnO_2/PAni–20 nanocomposite showed a weight loss of 3% up to 100 °C due to the evaporation of residual water from the surface of the material. They showed a weight loss of 40% from 100 to 1000 °C. Therefore, total weight loss for MnO_2/PAni–20 sample was 43%. Therefore, the quantity of PAni in the composite samples is 21% by weight which is very close to the amount PAni expected to be present in the MnO_2/PAni–20 nanocomposite. As a result, the TG analysis not only confirmed the formation of the nanocomposite but also revealed how much PAni was present in the MnO_2/PAni–20 nanocomposite.

CONCLUSIONS

Simple methods were carried out for the preparation of MnO_2, PAni, and MnO_2/PAni nanocomposites. The synthetic method was simple, economical friendly, consumes less time, free from hazardous materials. MnO_2, PAni, and MnO_2/PAni nanocomposites were prepared *via* hydrothermal, chemical oxidative polymerization, and ultrasonication method. Following the successful preparation of materials and nanocomposites, the samples were characterized using relevant sophisticated techniques. TEM micrographs show that MnO_2 particles produced were rod-like morphology and a size of approximately 37 nm. The obtained PAni is in emeraldine salt form which is the only conductive form of PAni. There was a special interaction between MnO_2 and PAni in the MnO_2/PAni composites. TG analysis was revealed the MnO_2/PAni nanocomposites contained the expected amount of PAni. The development of effective catalysts for the degradation of organic dyes dissolved in aqueous solution is hoped to favour from these obtained materials.

ACKNOWLEDGMENTS

This research work was supported by the **Bose Center for Advanced Study and Research in Natural Sciences**, University of Dhaka, Dhaka-1000, Bangladesh.

REFERENCES

[1] Siddique, Hafiz Muhammad Abubakar, and Adiqa K. Kiani. "Industrial pollution and human health: evidence from middle-income countries." *Environmental Science and Pollution Research* 27 (2020): 12439-12448.

[2] Molinari, R., F. Pirillo, M. Falco, V. Loddo, and L. Palmisano. "Photocatalytic degradation of dyes by using a membrane reactor." *Chemical Engineering and Processing: Process Intensification* 43 (2004): 1103-1114.

[3] Inyinbor Adejumoke, A., O. Adebesin Babatunde, P. Oluyori Abimbola, A. Adelani Akande Tabitha, O. Dada Adewumi, and A. Oreofe Toyin. "Water pollution: effects, prevention, and climatic impact." *Water Challenges of an Urbanizing World* 33 (2018): 33-47

[4] Hossain, Md, Md Pabel, and Md Islam. "Fenton-Like Processes for the Removal of Cationic Dyes." In *Advanced Oxidation Processes in Dye-Containing Wastewater*, 29-89. Springer, Singapore, 2022.

[5] Hossain, Md Saddam, M. Yousuf A. Mollah, Md Abu Bin Hasan Susan, and Md Mominul Islam. "Role of in situ electrogenerated reactive oxygen species towards degradation of organic dye in aqueous solution." *Electrochimica Acta* 344 (2020): 136146-136153.

[6] Farhana, Tamanna Ishrat, M. Yousuf Ali Mollah, Md Abu Bin Hasan Susan, and Md Mominul Islam. "Catalytic degradation of an organic dye through electroreduction of dioxygen in aqueous solution." *Electrochimica Acta* 139 (2014): 244-249.

[7] Selvakumar, Karuppiah, Sakkarapalayam Murugesan Senthil Kumar, Rangasamy Thangamuthu, Kruthika Ganesan, Palanichamy Murugan, Parasmani Rajput, Shambhu Nath Jha, and Dibyendu Bhattacharyya. "Physiochemical investigation of shape-designed MnO2 nanostructures and their influence on oxygen reduction reaction activity in alkaline solution." *The Journal of Physical Chemistry C* 119 (2015): 6604-6618.

[8] Zhu, Qian, Jingping Hu, Bingchuan Liu, Shaogang Hu, Sha Liang, Keke Xiao, Jiakuan Yang, and Huijie Hou. "Recent advances on the development of functional materials in microbial fuel cells: from fundamentals to challenges and outlooks." *Energy & Environmental Materials* 5 (2022): 401-426.

[9] Pei, Chengang, Ruifu Ding, Xu Yu, and Ligang Feng. "Electrochemical oxygen reduction reaction performance boosted by N, P doped carbon layer over manganese dioxide nanorod." *ChemCatChem* 11 (2019): 4617-4623.

[10] Wu, Dajun, Shaohui Xu, Chi Zhang, Yiping Zhu, Dayuan Xiong, Rong Huang, Ruijuan Qi, Lianwei Wang, and Paul K. Chu. "Three-dimensional homo-nanostructured MnO 2/nanographene membranes on a macroporous electrically conductive network for high performance supercapacitors." *Journal of Materials Chemistry A* 4 (2016): 11317-11329.

[11] Zhang, Yuefang, Jia Liu, Yahong Zhang, Jin Liu, and Yuping Duan. "Facile synthesis of hierarchical nanocomposites of aligned polyaniline nanorods on reduced graphene oxide nanosheets for microwave absorbing materials." *RSC Advances* 7 (2017): 54031-54038

[12] Yang, Ruizhi, Zhaoxiang Wang, Lei Dai, and Liquan Chen. "Synthesis and characterization of single-crystalline nanorods of α-MnO_2 and γ-MnOOH." *Materials Chemistry and Physics* 93 (2005): 149-153.

[13] Vijayalakshmi, S., E. Kumar, and S. Nithya. "Investigation on polyaniline with manganese dioxide nanostructure by using an in situ oxidative polymerization method." *Ionics* 26 (2020): 839-848

[14] Sun, Yin, Naibao Huang, Xiannian Sun, Dongchao Wang, Junjie Zhang, Shaoming Qiao, and Zhaoqing Gao. "An improvement on capacitive properties of clew-like MnO_2 by thermal treatment under nitrogen." *International Journal of Hydrogen Energy* 42 (2017): 20016-20025.

Dr. Md. Mominul Islam
Professor
Department of Chemistry
University of Dhaka
Dhaka-1000

28/03/23